Axon initial segment cytoskeleton comprises a multiprotein submembranous coat containing sparse actin filaments

Steven L. Jones, Farida Korobova, and Tatyana Svitkina

Department of Biology, University of Pennsylvania, Philadelphia, PA 19104

The axon initial segment (AIS) of differentiated neurons regulates action potential initiation and axon–dendritic polarity. The latter function depends on actin dynamics, but actin structure and functions at the AIS remain unclear. Using platinum replica electron microscopy (PREM), we have characterized the architecture of the AIS cytoskeleton in mature and developing hippocampal neurons. The AIS cytoskeleton assembly begins with bundling of microtubules and culminates in formation of a dense, fibrillar–globular coat over microtubule bundles. Immunogold PREM revealed that the coat contains a network of known AIS proteins, including ankyrin G, spectrin βIV, neurofascin, neuronal cell adhesion molecule, voltage-gated sodium channels, and actin filaments. Contrary to existing models, we find neither polarized actin arrays, nor dense actin meshworks in the AIS. Instead, the AIS contains two populations of sparse actin filaments: short, stable filaments and slightly longer dynamic filaments. We propose that stable actin filaments play a structural role for formation of the AIS diffusion barrier, whereas dynamic actin may promote AIS coat remodeling.

Introduction

The axon initial segment (AIS) is a specialized compartment of polarized neurons that separates the somatodendritic domain from the axonal domain. The AIS functions as the site of synaptic input integration and action potential initiation because of high density clustering of voltage-gated ion channels (Kole et al., 2008). The AIS is also a major contributor to the maintenance of axon–dendrite polarity that is critical for establishment of the entire neuronal circuitry (Hedstrom et al., 2008; Sobotzik et al., 2009; Song et al., 2009). Neuronal injury can alter the properties of the AIS, whereas mutations in AIS proteins may contribute to pathogenesis of neurological disorders, such as epilepsy and schizophrenia (Buffington and Rasband, 2011; Kole and Stuart, 2012). Although much is known about its role in action potential initiation, it remains less clear how the AIS maintains neuron polarity, partly because of poor understanding of its cytoskeletal architecture.

Early electron microscopy studies using a thin-section technique revealed microtubule (MT) fascicles and a dense granular undercoating at the plasma membrane as two characteristic features of the AIS (Palay et al., 1968). Later studies showed clustering of various membrane and submembranous proteins, such as ankyrin G (AnkG; Kordeli et al., 1995), spectrin βIV (Berghs et al., 2000), voltage-gated ion channels (Devaux et al., 2004; Kole et al., 2008), and cell adhesion molecules (Davis et al., 1996), within the AIS that could correspond to the membrane undercoating. The adaptor protein AnkG is one of the earliest components localized to the AIS and is responsible for the recruitment of most other AIS-enriched proteins (Zhou et al., 1998; Jenkins and Bennett, 2001; Hedstrom et al., 2007) and for maintaining AIS structure and role in neuron polarity (Zhou et al., 1998; Hedstrom et al., 2008; Sobotzik et al., 2009).

AIS contribution to neuron polarity depends on formation of a barrier that prevents diffusional mixing of plasma membrane components between axons and dendrites (Kobayashi et al., 1992; Nakada et al., 2003; Song et al., 2009). This AIS function depends on actin cytoskeleton dynamics (Winckler et al., 1999; Nakada et al., 2003; Song et al., 2009),

Correspondence to Tatyana Svitkina: svitkina@sas.upenn.edu

Abbreviations used in this paper: AIS, axon initial segment; AnkG, ankyrin G; DIV, days in vitro; LatB, latrunculin B; MT, microtubule; NrCAM, neuronal cell adhesion molecule; Nav, voltage-gated sodium channel; PEG, polyethylene glycol; PREM, platinum replica electron microscopy; RBC, red blood cell; S1, subfragment 1.

The Rockefeller University Press $30.00
J. Cell Biol. Vol. 205 No. 1 67–81
www.jcb.org/cgi/doi/10.1083/jcb.201401045

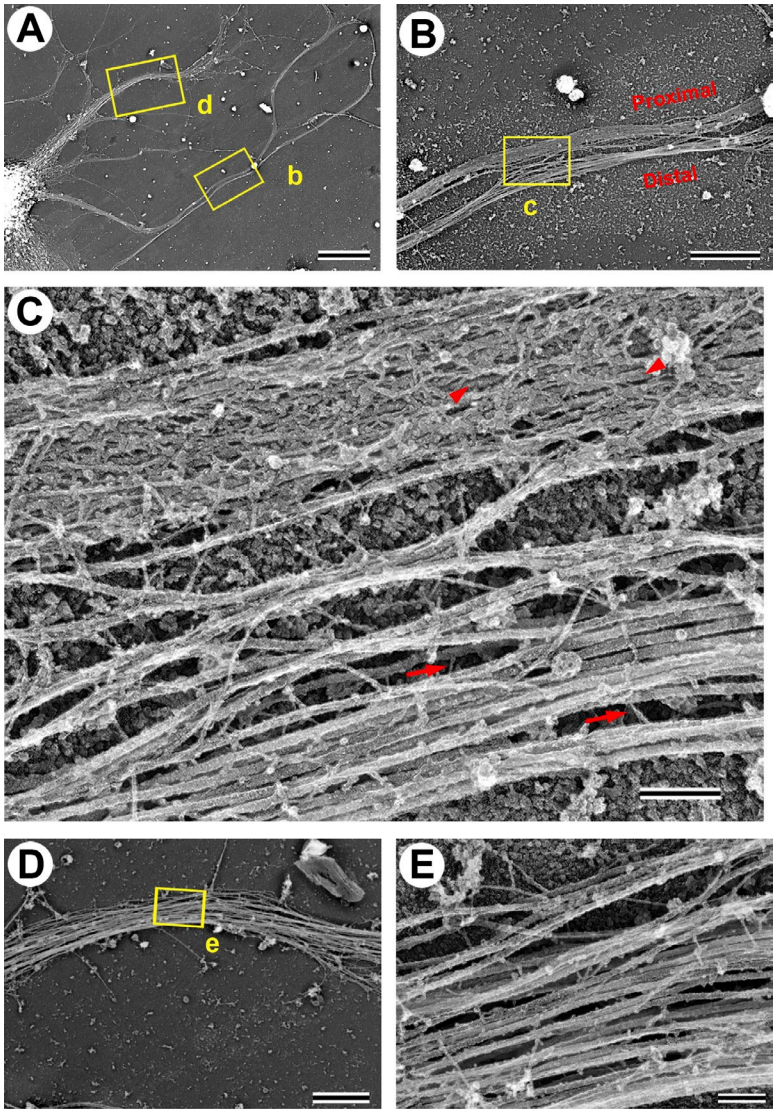

Figure 1. **Structure of the cytoskeleton in neuronal processes of DIV7 hippocampal neurons.** (A) PREM of a portion of the neuron with dendrites (e.g., box d) and an axon (box b) extending from the soma (bottom left). The axon forms a loop, so that proximal and distal segments can be seen next to each other (box b). (B and C) Sequential enlargements of box b in A showing exposed MTs with occasional thin fibrils (arrows) in the distal axon (bottom segment) and a fibrillar coat over MTs (arrowheads) in the proximal axon (top segment). (D and E) Sequential enlargements of box d in A showing dendrite cytoskeleton that lacks a fibrillar coat. Bars: (A) 10 µm; (B and D) 2 µm; (C and E) 200 nm.

but the specific role of actin remains unclear. Several models have been proposed to explain the phenomenon. The picket fence model suggests that a dense submembranous actin meshwork in the AIS physically obstructs diffusion of plasma membrane proteins (Kusumi et al., 2012). Another model proposes that oriented actin tracks mediate polarized trafficking of vesicular cargo across the AIS in a myosin Va– and myosin VI–dependent manner (Al-Bassam et al., 2012; Watanabe et al., 2012). Additionally, analysis of the distribution of several cytoskeletal proteins by subdiffraction fluorescence microscopy suggested that axons contain actin–spectrin networks (Xu et al., 2013) analogous to those in red blood cells (RBCs; Byers and Branton, 1985; Mohandas and Gallagher, 2008). However, this model does not explain a role for actin dynamics in neuron polarity, because short actin filaments connecting spectrin molecules at junctional complexes in RBCs are extensively stabilized by tropomyosin and capping proteins (Fowler, 1996; An et al., 2007). Thus, characterization of the high resolution structure of the AIS actin cytoskeleton has potential to shed light on these conflicting views about the mechanisms of neuron polarity.

Here we used platinum replica electron microscopy (PREM) to determine the molecular architecture of the AIS, with a special focus on the actin cytoskeleton, in dissociated hippocampal cultures at different stages of neuronal development. Our data reveal novel features of AIS architecture essential for understanding its assembly and functions.

Results

The AIS cytoskeleton comprises a dense submembranous coat

To determine the structure of the AIS cytoskeleton, we used PREM of detergent-extracted hippocampal neurons cultured for 7 d in vitro (DIV7; Fig. 1), when the AIS is considered to become fully assembled (Grubb and Burrone, 2010). Axons in these fully polarized neurons were distinguished from dendrites by their extended length. The cytoskeleton of both axons and dendrites largely consisted of MTs associated with few thin (3–6-nm) fibers that often appeared to cross-link the MTs and also included few neurofilaments (Fig. 1, C and E). The proximal axon of most neurons, however, had an unusual cytoskeletal structure characterized

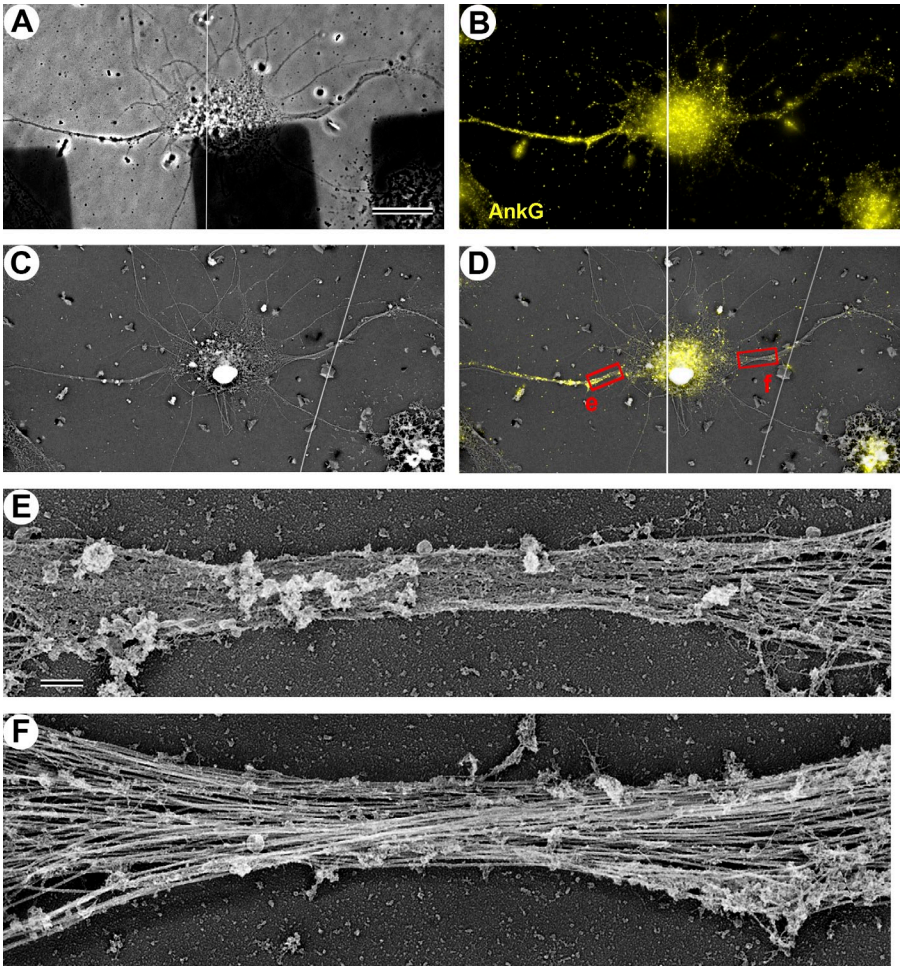

Figure 2. **Fibrillar coat is specific for AnkG-positive AIS.** (A–D) Correlative phase-contrast (A), immunofluorescence (B), and PREM (C) of a DIV10 neuron stained with AnkG antibody (yellow). AnkG-positive axon extends to the left and AnkG-negative major dendrite extends to the right. B and C are combined in D. (D) Boxes e and f are enlarged in panels E and F, respectively, to show a dense coat in the AnkG-positive proximal axon (E) but not in the AnkG-negative axon hillock (E, right), nor in the proximal dendrite (F). Bars: (A–D) 20 µm; (E and F) 0.5 µm. The images in A and B are composites of two partially overlapping frames. White lines in A and B and the overlay in D indicate the boundary between the individual images.

by the presence of a fibrillar network (subsequently referred to as "coat") of variable density that appeared to cover MTs, rendering them mostly hidden when the coat density was especially high (Fig. 1, A–C). Yet, MTs still spanned this region as revealed by immunofluorescence staining of neuron-specific tubulin β3 isoform (see Fig. 6). The structural difference between proximal and distal axons was especially clear in an example where the axon looped during its trajectory, offering a side-by-side view of proximal and distal segments of the same axon (Fig. 1, A–C). Within an individual axon, the coat density typically diminished toward the ends of the coated region and was undetectable in the axon hillock or in the distal axon. The position (starting at ∼5–25 µm from the soma) and the length (∼30–60 µm) of the coated regions in proximal axons match those known for the AIS (Sloper and Powell, 1979; Duflocq et al., 2011; Galiano et al., 2012; Kole and Stuart, 2012), suggesting that the coat is a characteristic feature of the AIS. We confirmed this suggestion by immunofluorescence staining of AnkG followed by correlative PREM of the same DIV7 neurons (Fig. 2, A–D). This approach revealed that the AnkG-positive region of the proximal axon contained a dense coat, which was virtually absent from the axon hillock (Fig. 2, D and E), dendrites (Fig. 2, D and F), and distal axon (not depicted), where AnkG immunofluorescence was diminished. These data demonstrate that the submembranous fibrillar coat is a specialized component of the AIS.

Assembly of the AIS coat during neuronal development

To understand how the AIS cytoskeleton assembles during neuronal maturation at a structural level, we examined the proximal axon by PREM from DIV3 to DIV21 (Fig. 3). In early DIV3 or DIV4 cultures (Fig. 3, A and B), few axons (longest neurites) contained a fibrillar coat in the proximal region (within 100 µm from the hillock; Fig. 3 G). Instead, most early axons (64%) displayed tight MT bundles, either continuous or intermittent (Fig. 3 B and Fig. S1), which were not observed in distal axon regions. Actin filaments were sparse in axons along most of their length, but abundant in the distal axon, growth cones, and occasional lateral protrusions, such as filopodia and patches (Gallo, 2013; Fig. S2).

At DIV7, ∼80% of neurons displayed in their proximal axons a fibrillar coat mixed with occasional globules of various shapes and sizes (Fig. 3, C and G). The density of the coat varied broadly, from sparse fibrils with variable thicknesses (3–11 nm) and orientations (Fig. 3 C) to dense networks (Figs. 1 and 2). By DIV10 and DIV14, the density of the coat progressively increased and coat substructure gradually shifted from fibrillar to globular (Fig. 3, D, E, and G). In proximal axons at DIV21, the coat was dominated by tightly packed globules that completely covered the MTs (Fig. 3, F and G). However, fibrils were also occasionally observed in small spaces between globules (Fig. 3 F).

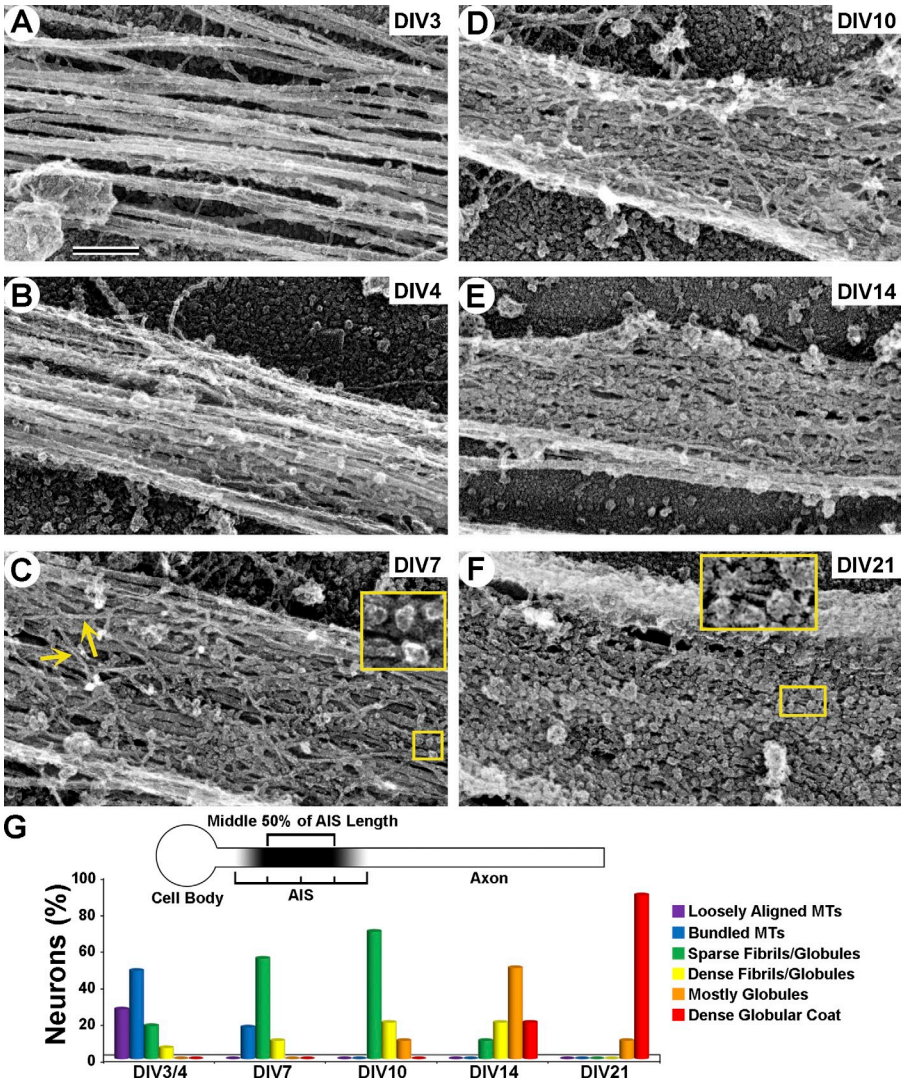

Figure 3. **Assembly of the AIS coat during neuron maturation.** (A–F) Representative PREM images of proximal axons showing their typical structural features at indicated DIV. (A and B) Loosely aligned (A) or bundled (B) MTs. (C) Loose fibrillar (arrows) coat containing sparse globules (inset). (D) Dense fibrillar–globular coat. (E) Dense mostly globular coat with some fibrils. (F) Mature mostly globular coat with some thin parallel fibrils (inset). Bar, 200 nm. (G) Categorization of proximal axons based on prevalent structural features within the middle 50% of AIS length, where coat density is most uniform (top, diagram). Graph shows the percentage of neurons in each category at different time points. DIV3/4, $n = 38$; DIV7, $n = 31$; DIV10, $n = 14$; DIV14, $n = 11$; DIV21, $n = 12$.

These fibrils were typically oriented along the axon axis, in contrast to variable orientation in younger neurons.

Thus, assembly of the AIS cytoskeleton initiates with formation of MT bundles (fascicles) at DIV3/4, followed by progressive accumulation of a fibrillar–globular coat over the MT bundles (DIV7–10) and a gradual shift in coat substructure from predominantly fibrillar to mostly globular (DIV14–21).

Actin filament organization in the AIS

Actin is essential for the AIS barrier function and may thus be a component of the coat. We first investigated organization of actin in the AIS of DIV3–21 hippocampal neurons by fluorescence microscopy. Staining of directly fixed or preextracted neurons gave similar results. At all ages, phalloidin staining within the AnkG-positive AIS was weak and diffuse except for few bright diffraction-limited puncta (Fig. 4, A and B). DIV7–21, but not DIV3, neurons displayed a slightly higher mean F-actin content within AISs, relative to distal axon regions adjacent to the AIS (Fig. 4 C). This increase was likely attributable to slightly increased number of actin puncta in the AIS of older neurons (Fig. 4, A and B).

We next used PREM to define actin organization in the AIS of DIV10 neurons, when the coat is sufficiently dense, but still mostly fibrillar. Although actin filaments can be identified in PREM samples based on their thickness or using myosin subfragment 1 (S1) decoration, very short filaments may escape detection by either approach. Therefore, we used immunogold PREM to detect phalloidin-stained actin filaments with an antibody to the phalloidin-bound fluorophore. This labeling approach was both specific and complete, resulting in virtually full coverage of detectable actin filaments with gold particles in actin-rich protrusions, whereas MTs were unlabeled (Fig. S3). In contrast, in the AIS of DIV10 neurons, the level of immunogold labeling was low, consistent with fluorescence microscopy data. The immunogold patterns could be divided into two categories. Some gold particles were linearly arranged along actin filaments 330 ± 242 nm (mean ± SD) in length and others were distributed as single particles or in small clusters (Fig. 5 A), indicative of very short phalloidin-labeled actin filaments that could be analogous to short filaments in RBCs.

To obtain a clearer view of the AIS cytoskeleton, we examined axonal branch points. Neurons are known to form branches from their main axon shaft (Gallo, 2011). In our cultures, branches

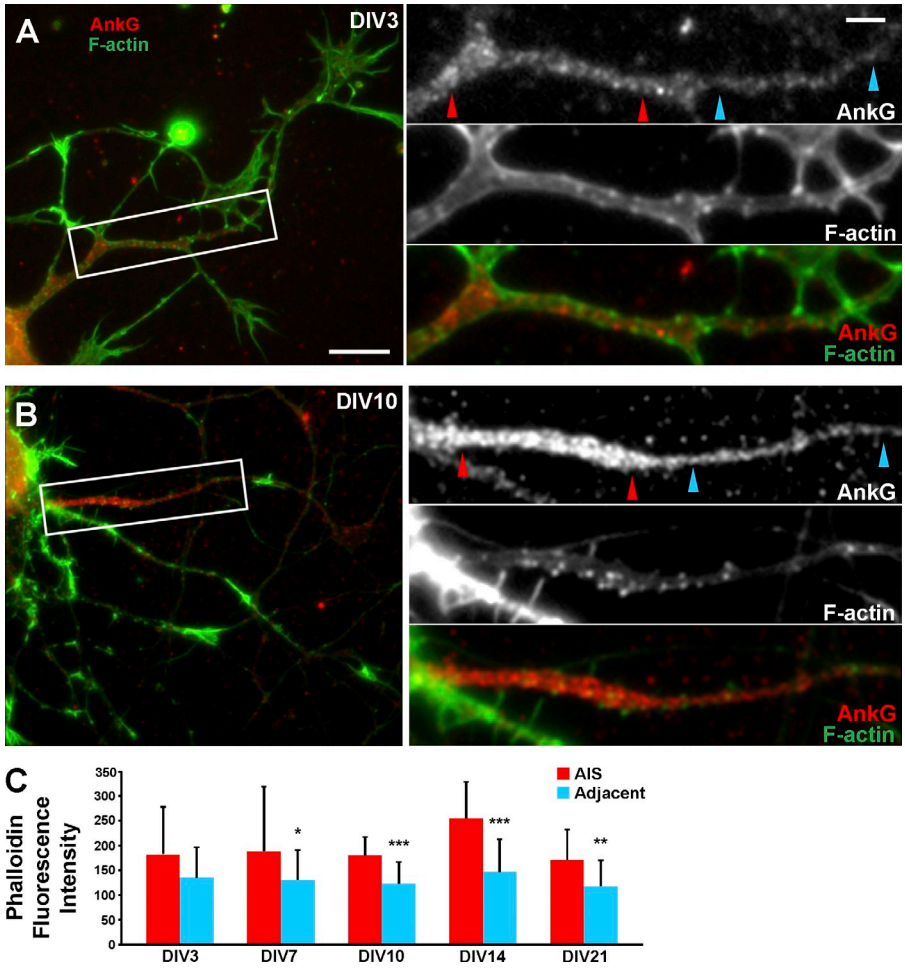

Figure 4. **Actin filament distribution in the AIS.** (A and B) DIV3 (A) and DIV10 (B) neurons stained with Alexa Fluor 488–phalloidin (F-actin) and AnkG antibody after detergent extraction. Boxes are enlarged on right and shown as individual channels and a merged image. Red and cyan arrowhead pairs mark the AIS and adjacent axonal region, respectively, as examples of how regions of interest were selected for quantification in C. (C) Quantitative analysis of mean phalloidin fluorescence intensity (in arbitrary units) within AnkG-positive AISs of DIV7–21 neurons, relative to distal axon regions immediately adjacent to the AIS. Data were analyzed using two-tailed, paired *t* test (n = 10 axons per age group). *, $P < 0.05$; **, $P < 0.01$; ***, $P < 0.001$. Error bars represent standard deviations. Bars: (A and B) 10 µm; (enlargements) 1 µm.

and actin-rich protrusions occasionally formed in the proximal axon (Fig. 5 B). Remarkably, the AIS coat covered not only the main axon, but also the beginning of the branch, and appeared to undergo "stretching" at branch junctions, suggesting that the coat has elastic properties. These stretched regions of the coat displayed fewer globules and more thin fibrils, than in the main axon (Fig. 5 B, b1). The fibrils were free of gold labeling and often oriented roughly in the direction of apparent stretch (Fig. 5 B, b2). These observations suggest that globules and fibrils in the AIS coat may partly represent the same molecules undergoing conformational change. An expanded coat at branch junctions could help to reveal more actin filaments in the AIS if their paucity was caused by poor penetration of labeling reagents. However, we observed approximately the same level and pattern of phalloidin gold staining as in shafts of main axons (Fig. 5, A and B).

To test an idea that actin filaments in the AIS can form directional tracks, we examined the orientation of actin filaments that had an appreciable length in DIV10 AISs using S1 decoration (Fig. 5 C). We found that filaments displayed no preferential orientation in the AIS (Fig. 5 D). Similar results were observed in DIV3 cultures (unpublished data). Together, these data suggest that actin filaments in the AIS coat are sparse and constitute two categories: very short filaments and slightly longer filaments with mixed orientation.

The AIS coat is a self-maintained scaffold

Major components of the AIS are resistant to detergent extraction and remain associated with the cytoskeleton (Garrido et al., 2003; Sánchez-Ponce et al., 2012), suggesting that they form a highly interlinked polymeric scaffold. However, dynamic actin filaments and/or MTs can play a role in maintaining coat integrity. Therefore, we examined effects of actin filament and/or MT depletion from DIV10 detergent-extracted neurons on AIS coat structure. Fluorescence microscopy showed a significant reduction of actin filaments after treatment of detergent-extracted cells with actin-severing protein gelsolin and of MTs after incubation of extracted cells in a cold calcium-containing buffer without altering AnkG staining (Fig. 6, A and B).

Phalloidin immunogold staining revealed the complete removal of long actin filaments after gelsolin treatment. However, many single or small clusters of gold particles were still present in the AIS coat, suggesting that short actin filaments are resistant to severing by gelsolin (Fig. 6 C, c1 and c2), possibly because of their interaction with stabilizing proteins in analogy to short actin filaments in RBCs. The AIS coat remained intact after gelsolin treatment in both main axonal shafts (Fig. 6 C, c1) and stretched regions (Fig. 6 C, c2). The coat structure also seemed well preserved after removal of MTs (Fig. 6 D) or after removal of both actin filaments and MTs (Fig. 6 E). These data indicate that the AIS coat maintains its structure independent of

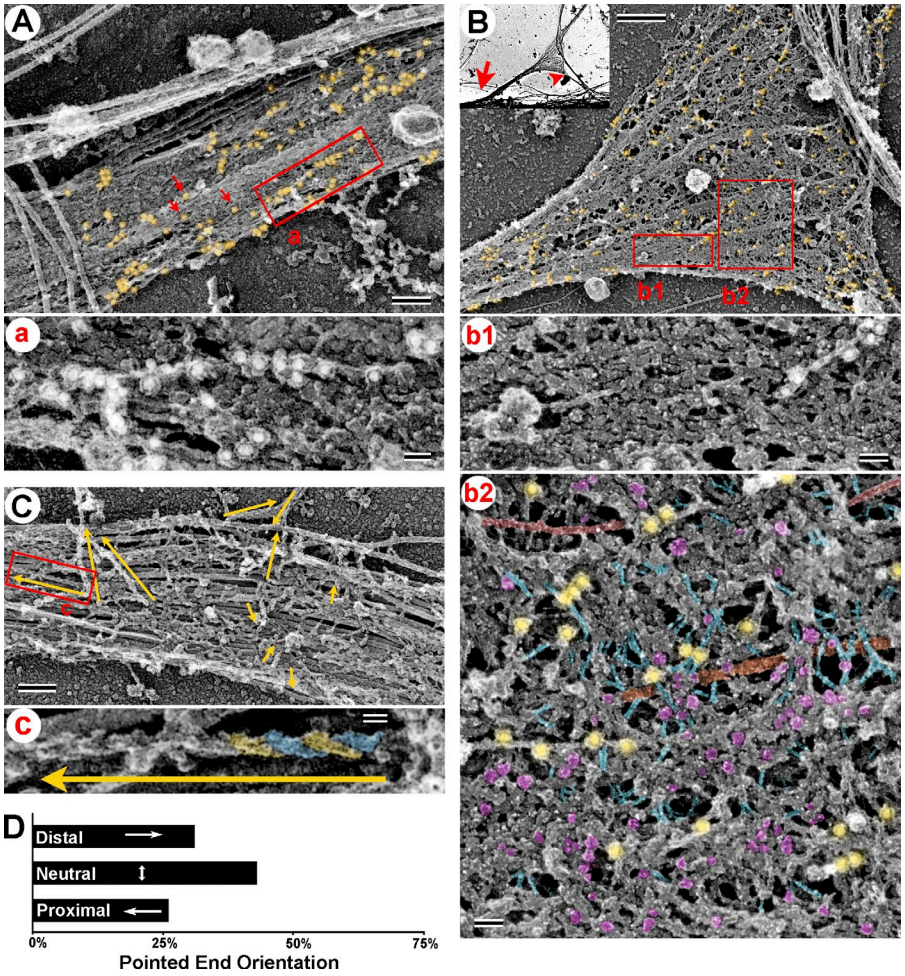

Figure 5. **Actin filament organization in the AIS.** (A and B) Immunogold PREM of actin filaments in DIV10 neurons. (A) The AIS coat along the main axon. Gold particles (18 nm; yellow shade) form linear arrangements (box a, enlarged in panel a) or appear as individual particles (red arrows) or small clusters. (B, inset) Axonal branch (arrowhead) emerging from the main axon (arrow) at the AIS. (B) Magnified branch junction with the AIS coat. Phalloidin immunogold is highlighted in yellow. (b1 and b2) Non-stretched (b1) and stretched (b2) regions of the AIS coat boxed in B. Selected fibrils (blue), globules (magenta), MTs (orange), neurofilaments (red), and phalloidin immunogold (yellow) are highlighted. (C) Decoration of actin filaments with myosin S1. Yellow arrows indicate filament lengths and direction of the pointed end. The boxed area is enlarged in panel c to show an S1-decorated filament with individual polar features highlighted in blue and yellow. (D) Quantification reveals unbiased orientation of actin filaments in the AIS. χ^2 (1, n = 181 from 10 AISs) = 0.786; P = 0.3752. Bars: (A and C) 200 nm; (B) 0.5 µm; (a, b1, and b2) 50 nm; (c) 20 nm.

MTs and long (~300-nm) actin filaments. However, short actin filaments may be required for coat structural integrity by functioning similar to junctional complexes in RBCs.

Latrunculin impairs coat spreading at axonal branch junctions

The role of actin in AIS barrier function was revealed by applying actin drugs to living cells (Winckler et al., 1999; Nakada et al., 2003; Song et al., 2009), which may be more disruptive for the AIS coat than depolymerization of actin in extracted neurons by gelsolin treatment. We used latrunculin B (LatB) treatment of DIV10 living neurons to further test a role for actin filaments in AIS coat structure. By fluorescence microscopy, LatB did not affect AnkG staining, but reduced phalloidin staining relative to DMSO controls (Fig. 7, A–C). This decrease was primarily because of a loss of actin filament puncta, whereas diffuse actin fluorescence within the AIS appeared only modestly affected (Fig. 7, A and B, bottom).

Consistently, phalloidin immunogold PREM revealed a strong reduction in linearly clustered gold particles (long actin filaments), suggesting that they are dynamic, whereas small clusters (short actin filaments) were largely preserved (Fig. 7, D and E), suggesting that they are stable. Similar to gelsolin-treated samples, no major changes were observed in the dense AIS coat along the axon shaft after LatB treatment (Fig. 7 D). However, at axonal branch junctions, the coat typically was not spread as observed under control conditions (Fig. 5 B) and appeared sparse with many large gaps (Fig. 7 E). In other cases, the AIS coat appeared to peel off the MT bundles as a cohesive sheet (Fig. S4). These data suggest that dynamic actin filaments contribute to AIS coat elasticity and potentially to its interaction with MT bundles.

Molecular architecture of the AIS coat

To further understand the molecular organization of the AIS coat, we wanted to identify major AIS components by immunogold PREM. As a first step toward this goal, we confirmed by immunofluorescence microscopy that spectrin βIV, the cell adhesion molecules neurofascin and neuronal cell adhesion molecule (NrCAM), and voltage-gated sodium channels (Nav) all remained enriched in the AnkG-positive AIS of DIV14 neurons after detergent extraction (Fig. 8, A–D), a procedure used to prepare samples for PREM.

Because of molecular and structural similarities between the AIS coat and RBC membrane skeleton, we tested whether the AIS contains adducin, a specific component of RBC cytoskeleton, which caps barbed ends of short actin filaments in the RBC junctional complexes and stabilizes actin–spectrin interaction (Kuhlman et al., 1996). Consistent with previous studies (Kaiser et al., 1989; Xu et al., 2013), we found that adducin

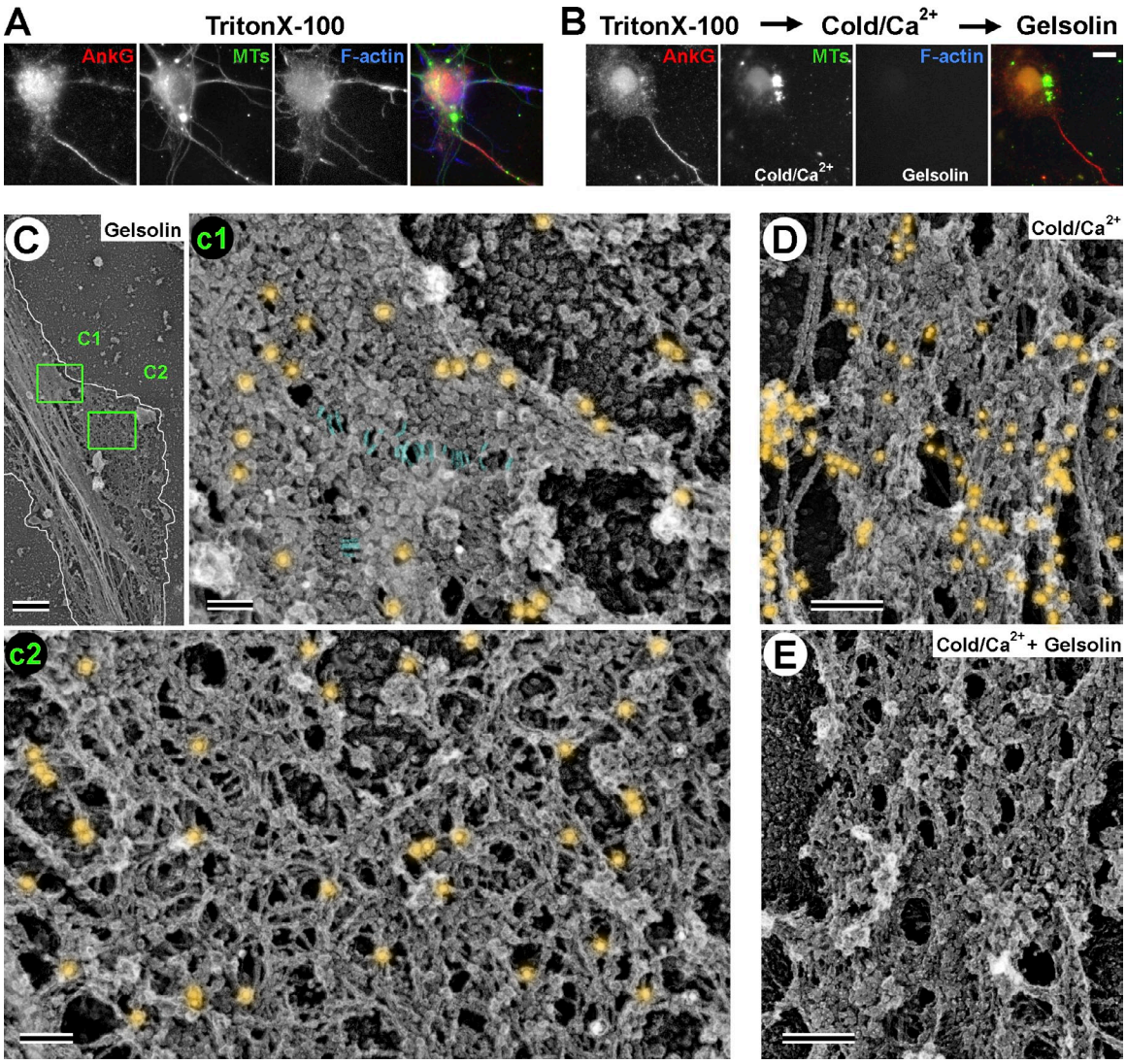

Figure 6. **Structure of AIS coat after actin filament and MT extraction.** (A and B) Fluorescence microscopy of detergent-extracted DIV10 neurons stained with Alexa Fluor 647–phalloidin (F-actin) and antibodies to AnkG and β3 tubulin (MTs). (A) Control neuron. (B) Neuron treated first with cold calcium-containing buffer to depolymerize MTs and then with gelsolin to sever actin filaments. (C–E) PREM of DIV10 neurons treated with gelsolin (C), cold calcium (D), or both (E) and stained with phalloidin immunogold (C and D). The AIS coat maintains integrity in all cases. (C) Low-magnification image of the proximal axon. White outline shows axon boundary. On the bottom right side, the coat spreads away from the axon shaft, probably being stretched by an actin-based protrusion removed by gelsolin treatment. Boxes c1 and c2 are enlarged in corresponding panels. (c1) Dense AIS coat along main axon and beginning of stretched region, where transversely oriented thin fibrils (blue) can be seen. (c2) Expanded coat at the putative branch junction contains numerous fibrils. Immunogold phalloidin staining in both c1 and c2 reveals only short filaments (i.e., individual particles and small gold clusters). (D) Dense coat in the axon shaft after MT depletion. Long, thick filaments are neurofilaments. Actin filament staining is comparable to that in untreated neurons (see Fig. 5 A). (E) Unstained AIS coat after removal of both actin filaments and MTs has fibrillar–globular structure similar to that in untreated neurons. Bars: (A and B) 10 µm; (C) 1 µm; (c1 and c2) 100 nm; (D and E) 200 nm.

immunofluorescence staining was present along dendrites and axons of DIV14 neurons. Surprisingly, however, adducin staining within the AIS was greatly diminished relative to other axonal regions (Fig. 8 E), suggesting that a mechanism of actin filament stabilization in the AIS is distinct from that in RBC junctional complexes despite structural similarities between AIS and RBC cytoskeletons. We next tested whether structural changes accompanying AIS maturation (Fig. 3) reflect different timing of arrival of various AIS components during AIS development. Immunofluorescence intensities of several AIS proteins (AnkG, spectrin βIV, neurofascin, NrCAM, and Nav) normalized to their respective maximal values over a period from DIV4 to DIV21 displayed a general upward trend (Fig. 8 F). However, neurofascin and especially NrCAM reached plateau relatively early, at DIV14 and DIV10, respectively, whereas spectrin βIV and Nav were recruited to the AIS with similar or slightly slower dynamics compared with AnkG, which is believed to recruit all other components to the AIS (Fig. 8 F). Thus, neurofascin and NrCAM could be responsible for the fibrillar appearance of the AIS coat in young neurons, whereas Nav channels likely contributed to accumulation of globular structures in the AIS of mature neurons. In contrast to these AIS proteins, adducin staining within the AIS revealed a downward trend between DIV6 and DIV21, suggesting that adducin is excluded from the AIS as it forms.

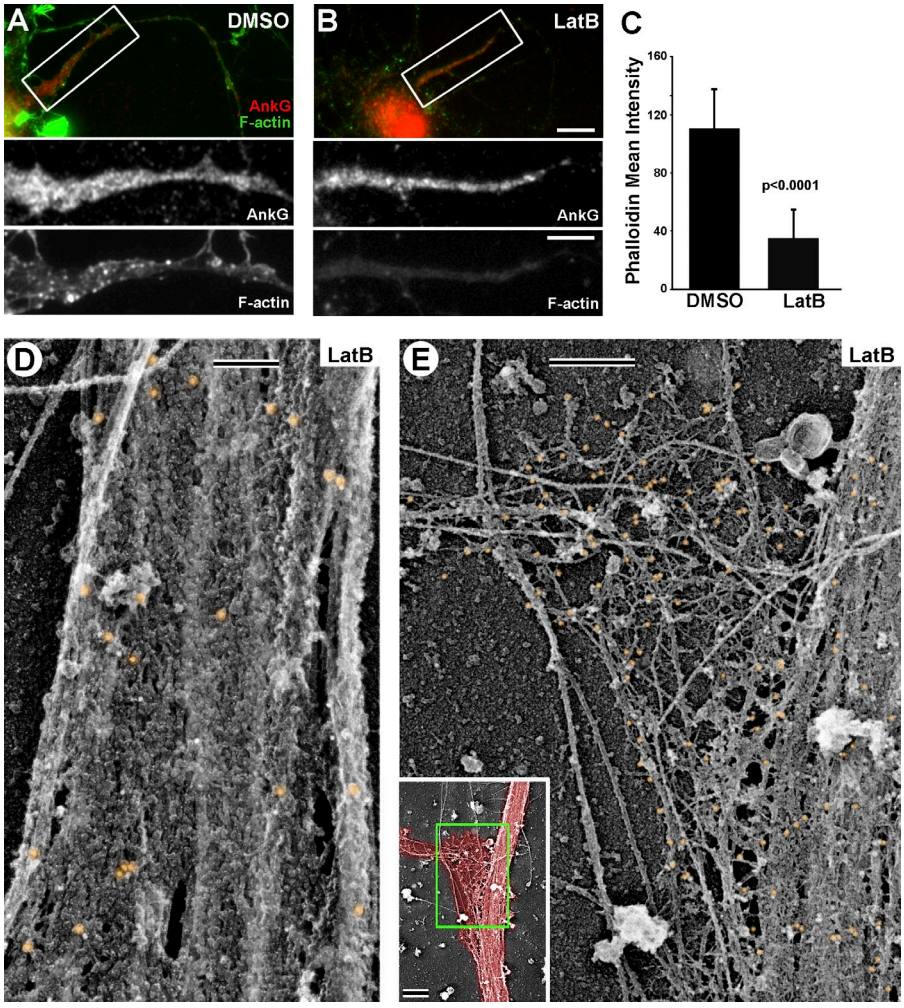

Figure 7. **Organization of AIS coat after LatB treatment.** (A and B) Fluorescence microscopy of DIV10 neurons stained with an AnkG antibody and Alexa Fluor 488–phalloidin (F-actin). Boxed regions are enlarged in bottom panels as individual channels. (A) Control DMSO-treated neuron. (B) Neuron treated with LatB (4 µM for 1 h). (C) Mean phalloidin fluorescence intensity in the AIS of DIV10 neurons after LatB or DMSO treatment. Data analyzed using Welch's *t* test (n = 10 axons per treatment group). Error bars represent standard deviations. (D and E) PREM of the AIS in LatB-treated DIV10 neurons after labeling with phalloidin immunogold. (D) The AIS coat at the axon shaft remains apparently intact and contains only short actin filaments (small gold clusters). (E) The AIS coat at the branch junction is sparse and disorganized, with large gaps. Inset shows an overview of this branch junction with axon area shaded in red and the zoomed region marked by green box. Bars: (A and B) 10 µm; (A and B, enlargements) 5 µm; (D and E) 200 nm; (E, inset) 1 µm.

To directly identify the AIS coat substructures, we used immunogold PREM with antibodies for several AIS proteins in DIV14 neurons, when both fibrils and globules are common. For all proteins examined, the identity of immunogold-associated structures in dense AIS regions was often ambiguous, requiring examination of regions where the coat was sparse or stretched. Accordingly, only a small fraction (~30%) of gold particles could be unambiguously interpreted.

Immunogold labeling of AnkG using an antibody against a C-terminally located epitope (Fig. 9) was positive in both fibril- and globule-rich regions of the coat (Fig. 9, A–D). Individual gold particles frequently labeled a tip of thin, often curved, filaments 139 ± 16 nm (mean ± SD) in length and 4.0–7.5 nm in width (Fig. 9 E). Other gold particles were associated with one end of elongated globular clusters of approximately the same length, but varying in shape and thickness throughout their lengths. These AnkG-based globular clusters could represent a thin flexible filament, like in the first category, associated with AnkG interaction partners.

Immunogold labeling of spectrin βIV, neurofascin, NrCAM, and Nav confirmed the presence of these proteins within the coat (Fig. 10, top). Individual spectrin βIV–positive structures comprised filaments 58 ± 20 nm in length (mean ± SD) and 4.5–6.5 nm in width that were either curved or fairly straight (Fig. 10, High Mag). They occasionally appeared to extend from elongated globular clusters (Fig. 10, bottom) analogous to those containing AnkG (Fig. 9). Individual neurofascin- and NrCAM-positive structures appeared as filaments that also sometimes bent (Fig. 10, high mag). Neurofascin filaments were 58 ± 24 nm in length (mean ± SD) and 6.0–6.5 nm in width, similar to reported dimensions of purified neurofascin molecules (Davis et al., 1993), whereas NrCAM filaments were longer (145 ± 23 nm) and slightly thicker (7.5–9.5 nm), which was unexpected because both neurofascin and NrCAM have similar molecular masses (186 and 145 kD, respectively).

Individual structures labeled by a pan-Nav antibody were globular or donut shaped with a 12.5 ± 2.3-nm (mean ± SD) diameter (Fig. 10, high mag), similar to that of purified protein (Sato et al., 2001). These Nav channels often clustered with other donut shapes of similar or larger (17.7 ± 1.5 nm, mean ± SD) diameter (Fig. 10, yellow arrows), possibly representing Nav proteins that were not immunolabeled or other channels known to localize to the AIS (e.g., potassium or calcium channels). Remarkably, similar donut shapes were sometimes apparent as components of AnkG-positive elongated globular clusters (Figs. 9 and 10) or in close proximity to NrCAM filaments (Fig. 10), consistent with known ability of Nav channels to interact with these proteins (Zhou et al., 1998; Lemaillet et al., 2003; McEwen and Isom, 2004; McEwen et al., 2004). Consistent

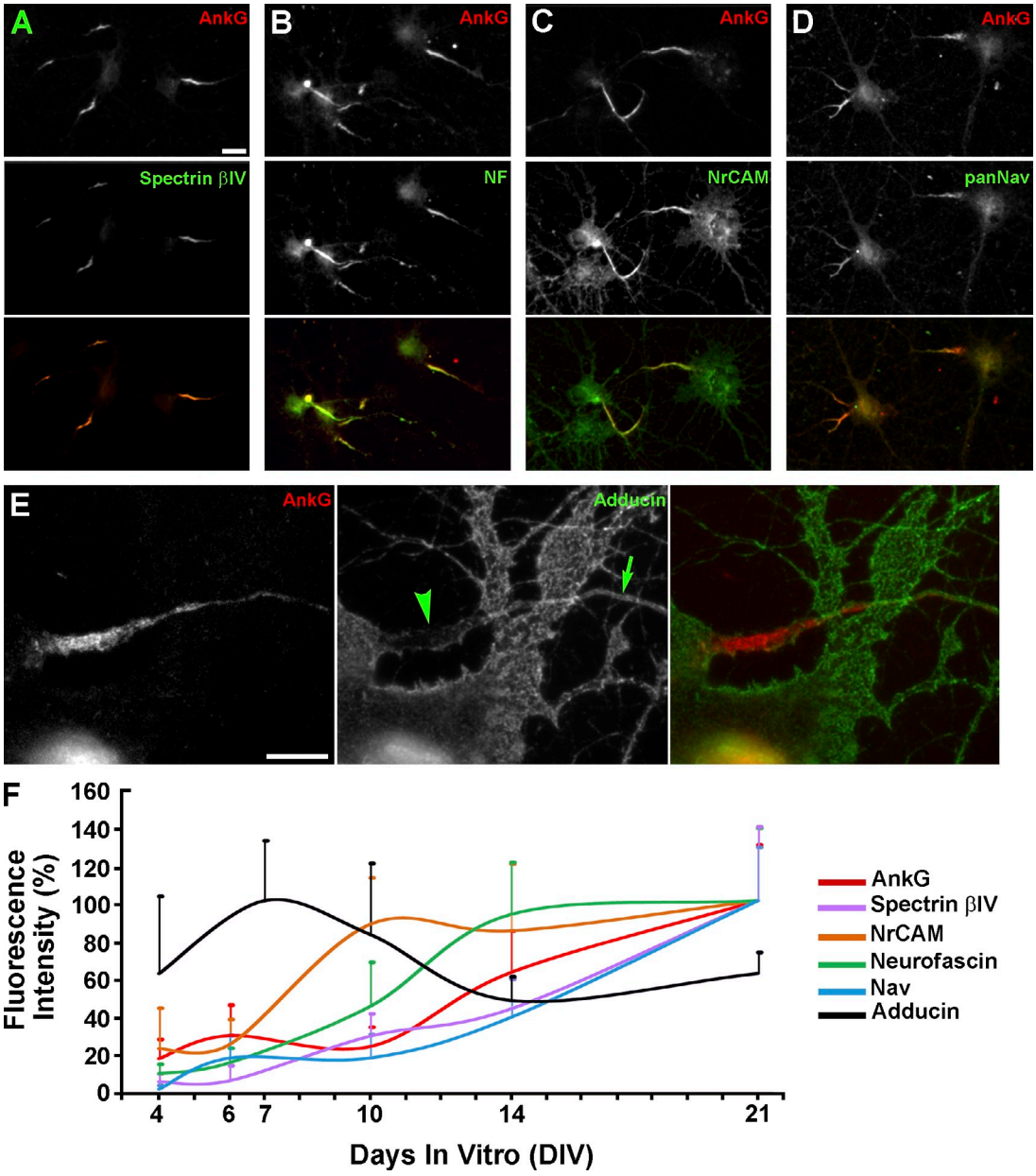

Figure 8. **Time course of accumulation of AIS proteins during neuron development.** (A–D) Major AIS proteins remain associated with the cytoskeleton after detergent extraction of DIV14 neurons and colocalize with AnkG. (E) Adducin is largely absent from the AnkG-containing AIS (arrowhead), but is abundant in dendrites and in the axon outside of the AIS (arrow). (F) Time course of protein accumulation in the AIS during neuronal development. Fluorescence intensities of individual immunostained proteins are expressed as a percentage of the maximal value over a period from DIV4 to DIV21 (DIV7 for adducin and DIV21 for other proteins) and plotted against the DIV. *n* values for DIV4, DIV6/7, DIV10, DIV14, and DIV21 are, respectively: 21, 29, 38, 36, and 51 for spectrin βIV; 9, 18, 28, 26, and 34 for NrCAM; 22, 37, 24, 46, and 32 for neurofascin; 36, 29, 27, 28, and 64 for Nav; and 98, 123, 127, 146, and 190 for AnkG. For adducin, *n* = 10 for DIV4–14 and 9 for DIV21. Error bars represent standard deviations. Bars: (A–D) 20 µm; (E) 10 µm.

with immunofluorescence data, adducin was not found in the AIS coat by immunoPREM (unpublished data). These observations demonstrate that the AIS coat comprises many proteins that are known to localize to the AIS, and that these proteins, in part, account for the globules and fibrils observed in the coat.

Discussion

AIS coat substructure

The AIS is highly enriched with AnkG and spectrin βIV (Grubb and Burrone, 2010). The best characterized ankyrin- and spectrin-rich structure is the membrane skeleton in RBCs, which represents an elastic meshwork of α/β spectrin heterotetramers connected at their ends by short (~35-nm) actin filaments at so-called junctional complexes (Byers and Branton, 1985). Actin filaments in junctional complexes are capped at both ends and stabilized along the length by tropomyosin (Fowler, 1996; An et al., 2007). The actin–spectrin meshwork in RBCs is attached to the plasma membrane primarily by ankyrin R, which interacts with both spectrin and transmembrane proteins, but components of junctional complexes and spectrin itself also participate in membrane binding (Mohandas and Gallagher, 2008). In artificially

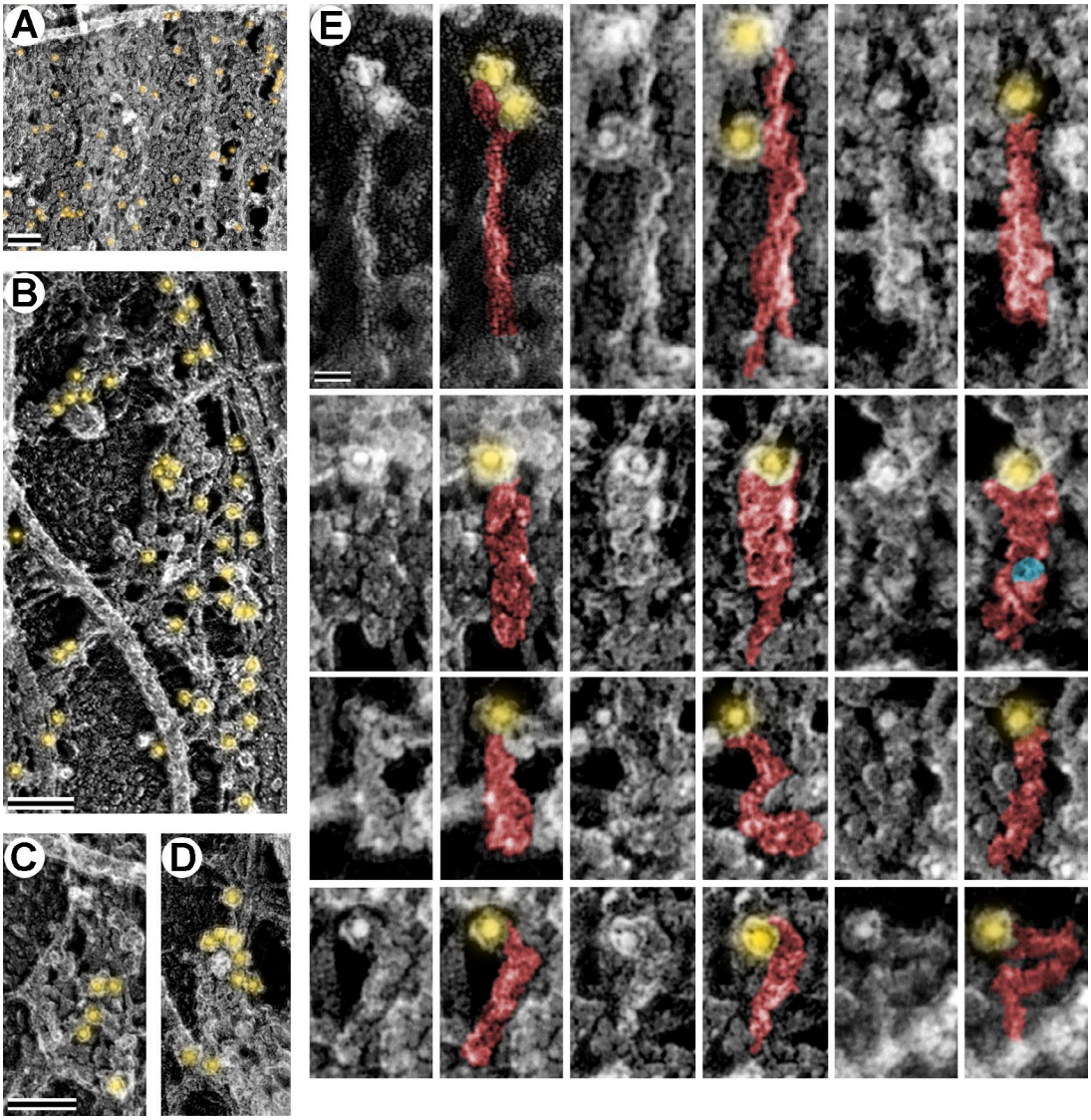

Figure 9. **AnkG organization in the AIS coat.** Immunogold PREM of AnkG in DIV14 neurons. (A–D) Regions of the AIS coat along the main axon. Gold particles (12 nm; yellow) are present in small clusters or individually in dense regions (A). In stretched or sparse regions of the coat, AnkG immunogold associates with fibrillar networks (B) or globular clusters (C and D). (E) A gallery of individual AnkG-positive structures in the sparse or stretched AIS coat. Duplicate images are pseudocolored to show gold particles (yellow) associated with putative AnkG structures (red), such as long, thin, wavy filaments (e.g., top row) or elongated globular clusters of variable thickness and morphology. A donut-shaped putative ion channel (see Fig. 10) within an AnkG globular cluster is pseudocolored in blue. Bars: (A–D) 100 nm; (E) 20 nm.

expanded RBC cytoskeletons, spectrin molecules are typically seen at their maximal length of ∼200 nm, whereas ankyrin R appears as globules along spectrin fibers (Byers and Branton, 1985). However, in native RBCs (Moyer et al., 2010; Nans et al., 2011) or platelets (Hartwig and DeSisto, 1991), the actin–spectrin meshwork appears more contracted, suggesting stress-dependent remodeling. Because spectrins and ankyrins are expressed ubiquitously, it is believed that similar actin–spectrin membrane skeletons provide structural support to the plasma membrane in other cell types. However, the structure of the membrane skeleton remained poorly characterized except in blood cells. In this study, we have extensively characterized the spatial and molecular architecture of the spectrin–ankyrin–rich submembranous cytoskeleton in the AIS of cultured hippocampal neurons and found both similarities and differences between the AIS coat and the RBC membrane skeleton.

The AIS coat appears structurally similar to native membrane skeletons in RBCs and platelets (Hartwig and DeSisto, 1991; Moyer et al., 2010; Nans et al., 2011), but displays more abundant globules, especially in the mature state. Our immuno-PREM data suggest that the majority of these globules can correspond to voltage-gated ion channels. Although we tested here only Nav channels, other channels that are abundant in the AIS likely contribute to the globular appearance of the AIS coat. Ion channels can also be responsible for the globular appearance of AnkG-positive elongated clusters, as most ion channels are recruited to the AIS through direct interaction with AnkG. A subset of globular structures may correspond to recoiled elongated molecules.

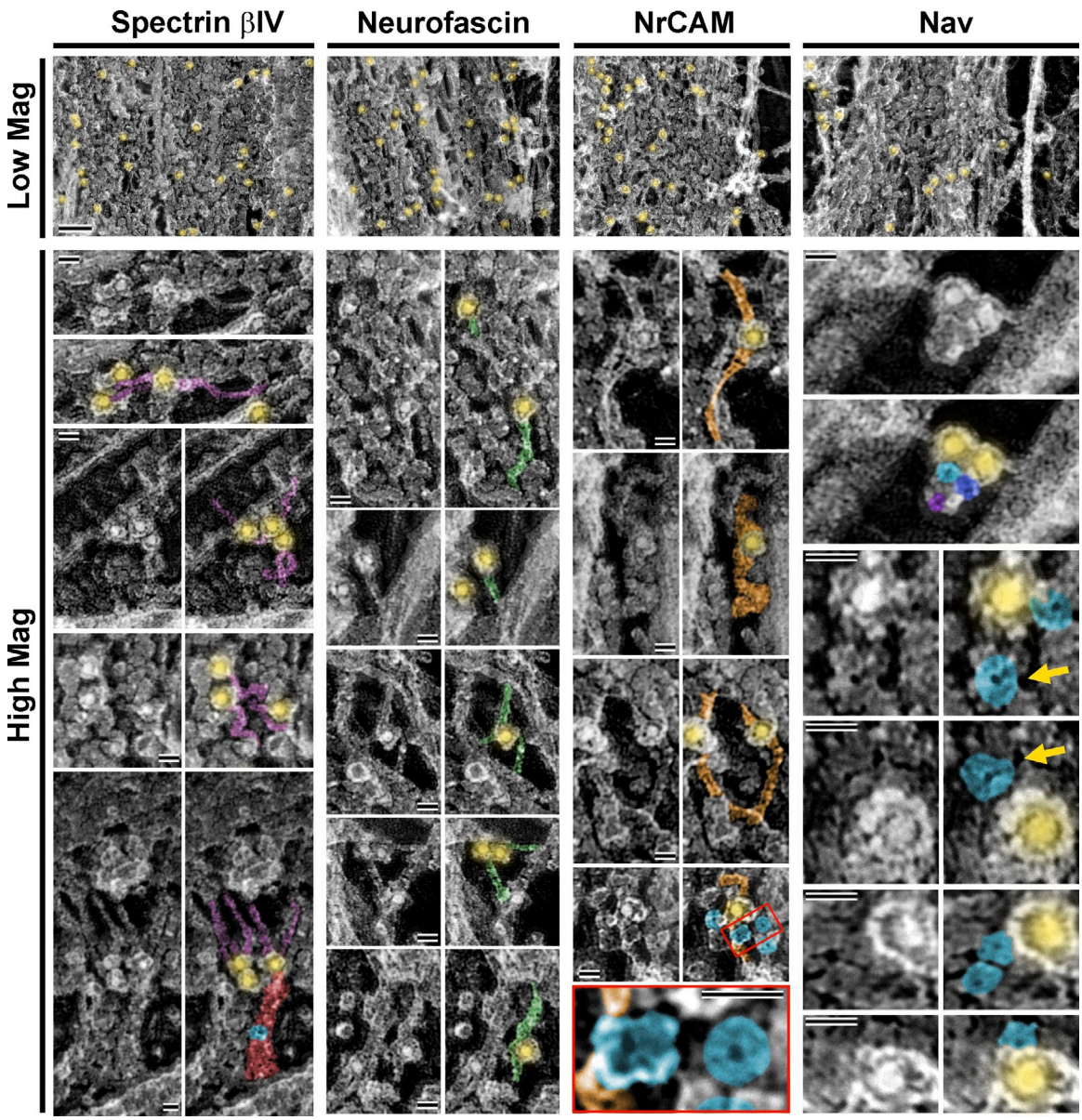

Figure 10. **Molecular composition of the AIS coat.** Immunogold PREM of indicated AIS proteins in DIV14 neurons. (Low Mag) Regions of dense AIS coats along the main axon shaft showing immunogold staining (yellow) of AIS proteins. Bar, 100 nm. (High Mag) Galleries of immunogold-stained AIS proteins in sparse or stretched regions of the coat. Duplicate images are pseudocolored to show gold particles (12 nm; yellow,) associated with putative spectrin βIV (violet), neurofascin (green), NrCAM (orange), and Nav (blue) proteins. A cluster of three putative Nav proteins (blue, purple, and magenta) associated with two gold particles is shown in the top right panel. Yellow arrows indicate donut-like shapes with slightly larger diameter than Nav, possibly representing other ion channels in the AIS. Several putative ion channels are in close proximity to an NrCAM-positive filament (enlarged in bottom panel from red box in the panel immediately above). Putative Nav-containing AnkG globular cluster is pseudocolored in red to highlight its close proximity to spectrin βIV (bottom left corner). Bars, 20 nm.

Thin fibrils found in the AIS coat represent a mixed population formed by neurofascin, NrCAM, and extended spectrin and AnkG molecules. Fibrillar appearance of neurofascin and NrCAM is consistent with the presence of six immunoglobulin repeats and three to five fibronectin repeats in their extracellular domains (Davis et al., 1993; Bennett and Baines, 2001). Although neurofascin and NrCAM, as well as ion channels, appear to be intermingled with cytoplasmic proteins, this impression is likely caused by the absence of the plasma membrane in PREM samples, rather than reflecting native intracellular localization of these transmembrane proteins. The filamentous appearance of AnkG is conceivable because the 480-kD AnkG isoform is predicted to have a flexible tail that may extend up to 0.5 µm from the globular membrane-binding head (Bennett and Healy, 2009). Fibrillar components of the AIS mostly run along the axon in mature AISs, but at axonal branch junctions, they acquire less uniform orientation, suggesting a forced rearrangement in response to tension exerted by the axonal branch. Although it remains unclear what force causes longitudinal alignment of fibers in the axon shaft and their reorientation at branch junctions, the fact that rearrangements are possible underscores the elastic nature of the AIS cytoskeleton and its ability to undergo

remodeling in a tension-dependent manner, similar to the membrane skeleton in RBCs (Nans et al., 2011).

Although we have identified several major components of the AIS coat, there are additional proteins that can contribute to the dense mass of fibrils and globules within the coat. They may represent several known AIS proteins (e.g., voltage-gated potassium or calcium channels or PSD93), as well as proteins that exist in the AIS but remain unknown. We also cannot exclude the possibility that the coat is partly impenetrable to gold particles, thereby underestimating the actual density of each protein.

Development of the AIS cytoskeleton

The specialized AIS skeleton is gradually assembled during neuron maturation with AnkG serving as a master organizer of the AIS (Bennett and Baines, 2001). Thus, it is expected that appearance of AnkG-based structures in the proximal axon should be a first sign of AIS assembly. Instead, we found that the first distinct feature of the proximal axon is MT bundling. In mature neurons, MT bundles become poorly visible by PREM as a result of high coat density, but they still span the AIS. MT bundles (fascicles) are a key signature of AISs in neurons (Palay et al., 1968). They may function as a filter for cytoplasmic proteins in mature AISs (Li et al., 2011) and to capture AIS structural components during AIS assembly.

The formation of MT bundles before arrival of AIS coat components does not contradict the idea of AnkG as a master organizer of the AIS. Indeed, AnkG itself can serve as a MT bundler during early stages of AIS development, because it can bind MTs and oligomerize (Bennett and Baines, 2001) and because AnkG knockout mice lack MT bundles (Sobotzik et al., 2009). Additional candidates to mediate MT bundling in the AIS are plus end–tracking proteins EB1 and EB3 because they (especially EB3) are enriched in the AIS, interact with AnkG, and induce MT bundles in a manner that is independent of plus end tracking (Leterrier et al., 2011).

A second feature of AIS assembly is accumulation of the fibrillar–globular meshwork that gradually coats MT bundles. The initial predominance of fibrils in the coat likely reflects accumulation of filamentous proteins that arrive early during AIS assembly, such as neurofascin, NrCAM, and, to a lesser extent, spectrin βIV. The subsequent accumulation of globules correlates with the late arrival of Nav channels and their donut-shaped morphology. Early arrival of neurofascin and NrCAM to the AIS is unexpected because neither of them is required for AIS assembly (Hedstrom et al., 2007), although neurofascin is needed for long term stabilization of the AIS and NrCAM clustering in mouse Purkinje cells (Zonta et al., 2011). Possibly, some early functions of these proteins in AIS assembly remain to be revealed.

Actin cytoskeleton organization in the AIS

We found two actin filament populations in the AIS: short stable filaments resistant to gelsolin or LatB treatment and longer dynamic filaments that are sensitive to these treatments. In RBCs, short actin filaments are connected by spectrin molecules within a regular triangular network (Byers and Branton, 1985). Subdiffraction fluorescence microscopy data suggested a similar actin–spectrin arrangement in axons of cultured neurons by showing that short adducin-positive actin filaments form periodic rings along the axon, including the AIS, and are connected by stretched and longitudinally aligned spectrin molecules (Xu et al., 2013). Although we indeed observed longitudinal fibrils in mature AISs, actin periodicity was not readily apparent in our phalloidin immunogold–stained samples. We doubt that actin rings were destroyed in our samples by detergent extraction because short actin filaments that supposedly form rings were sufficiently stable to survive not only extraction but also gelsolin or LatB treatment. Possibly, greater signal averaging combined with larger fields of view makes light microscopy better suited for revealing global features of actin organization, whereas higher resolution PREM can reveal small details.

We were also unable to document the presence of adducin in the AIS by light or electron microscopy, although it was readily detectable outside of the AIS. A reason for this discrepancy is currently unknown, especially because we used the same antibody and similar staining conditions. Regardless of these inconsistencies, because the periodic actin–spectrin arrangement detected by subdiffraction microscopy was observed throughout the axonal shaft and was not specific for the AIS, this structure unlikely plays a mechanistic role in the AIS polarity function. However, short actin filaments in the AIS can function similarly to junctional complexes in RBCs to maintain structural integrity of the coat.

In addition to short stable actin filaments, we also detected a small population of relatively long and dynamic actin filaments that were enriched by 30–50% in the AIS relative to adjacent axonal regions. In RBCs, short actin filaments in junctional complexes can be transiently uncapped and serve as seeds for polymerization of longer dynamic filaments (Byers and Branton, 1985), probably because adducin has relatively low affinity for barbed ends (Kuhlman et al., 1996). In the AIS coat, barbed ends of stable actin filaments should be capped by another barbed end capping protein, because adducin is not present there. However, these filaments can still be transiently uncapped in a regulated manner to serve as sites of actin polymerization to produce longer dynamic filaments.

Actin functions in the AIS

In cultured neurons, dynamic actin filaments are required for maintaining the AIS diffusion barrier (Winckler et al., 1999; Nakada et al., 2003; Song et al., 2009; Rasband, 2010). Because short actin filaments in the AIS are not dramatically affected by LatB treatment, we speculate that the dynamic actin filaments with submicrometer lengths are more likely to be responsible for LatB-dependent barrier defects. The spatial organization of the dynamic actin population in the AIS is essential to models of AIS polarity function. The polarized trafficking model (Al-Bassam et al., 2012; Watanabe et al., 2012) proposes that the AIS forms a selective filter that relies on oriented actin tracks present within 2–3-µm actin patches, which, however, were not correlated with AIS markers (Watanabe et al., 2012). We also observed 1–2-µm actin patches in axons, but they corresponded to actin-rich axonal protrusions rather than to AIS-specific structures. In contrast, the submicrometer-sized actin

puncta were constantly detected by fluorescence microscopy in the AIS. They likely corresponded to dynamic actin filaments in PREM images. These actin filaments, however, do not display preferential orientation and thus cannot serve as directional tracks in the AIS. These results, together with overall sparse distribution of actin filaments in the AIS, do not support a selective filter model that depends on polarized orientation of filaments.

The picket fence model proposes that a dense actin meshwork in the AIS prevents mixing of lipids and plasma membrane proteins between the axon and dendrites (Nakada et al., 2003; Kusumi et al., 2012), but supporting structural data are available only from epithelial cells (Morone et al., 2006). Our data reveal an actin network of insufficient density to hinder diffusion of membrane proteins in the AIS. Instead, the submembranous AIS coat could serve in this capacity, as it is very dense, even though not particularly rich in actin. Short stable actin filaments can contribute to the formation of the AIS diffusion barrier by maintaining the structural integrity of the coat.

The specific role of dynamic actin filaments in the maintenance of AIS-dependent neuron polarity is not entirely clear. A clue was provided by our observation that the most obvious structural aberrations in the AIS coat after LatB treatment occurred at axonal branch junctions. Because the AIS coat typically appears more stretched at branch junctions, we infer that the AIS coat may experience additional mechanical challenge at these sites, which may be tolerated in the presence of actin dynamics, but not in its absence. Thus, we propose that mechanical stress (or a chemical signal) induces coat remodeling that depends on dynamic actin filaments. For example, during remodeling events, spectrin and/or other AIS components may detach from actin filaments and then recombine into a new configuration. Long dynamic filaments can facilitate reassembly of the meshwork, for example, by capturing unattached spectrin molecules, whereas in their absence resealing of the coat can fail and cause meshwork rupture. In the absence of mechanical or chemical signals, however, dynamic actin filaments may be dispensable whereas short stable filaments serve exclusively to maintain coat integrity.

We assume that the remodeling capability of the AIS coat may be important for covering a branch junction, but it is likely even more essential for other events in the AIS, such as passage of vesicles through the crowded AIS. Thus, cases where the AIS coat peels off the MT bundles after LatB treatment may reflect the inability of the coat to reseal after vesicle passage. A need for remodeling may explain the selectivity of cargo transport, if we assume that an acceptable cargo carries a recognition signal, which initiates a remodeling process that transiently opens a passage for the cargo. It would be interesting to test this idea in the future, although is not the only scenario explaining LatB effects. Thus, dynamic actin filaments may participate in attaching the AIS coat to the plasma membrane and/or to MTs. It is also possible that global actin depolymerization triggers a mechanism for "opening" of the barrier to enhance supply of actin for other cellular activities, such as growth cone dynamics.

Conclusions

We used PREM to show that the AIS of mature neurons comprises a dense submembranous coat that is not present elsewhere in the neuron. We found neither a dense actin meshwork nor oriented tracks within the AIS, but revealed two subpopulations of actin: short stable and longer dynamic filaments. Although our data are in general consistent with the view that the AIS coat is analogous to that of the membrane skeleton of RBCs, we additionally revealed that dynamic actin filaments are important for providing remodeling capability to the AIS coat in stressed conditions. Based on this data, we propose that the dense fibrillar–globular coat functions as a diffusion barrier at the AIS to prevent mixing of axonal and dendritic proteins, whereas signal-triggered coat remodeling is dependent on dynamic actin filaments and allows for selective passage of vesicles during establishment of neuron polarity.

Materials and methods

Cell culture

Rat hippocampal cells (provided by M.A. Dichter, University of Pennsylvania, Philadelphia, PA) were isolated and dissected as described previously (Wilcox et al., 1994). In brief, hippocampi were dissected from brains of Sprague-Dawley rat embryos at embryonic day 18–20 and dissociated into individual cells by incubating in a trypsin-containing solution. The cells were then washed and plated at low density (60,000 cells/ml) on poly-L-lysine–coated (1 mg/ml) glass coverslips in 35-mm dishes in 1.5 ml neurobasal medium (Gibco) with 2% B27 supplement. AISs were analyzed at 3, 4, 7, 10, 14, and 21 DIV. LatB (EMD Millipore) was used at 4 µM prepared from a 1-mM stock solution in DMSO. Cultures were treated with LatB or DMSO (4%) for 1 h at 37°C.

Fluorescence microscopy

Cells were extracted with 1% Triton X-100 in PEM buffer (100 mM Pipes-KOH, pH 6.9, 1 mM $MgCl_2$, and 1 mM EGTA) containing 2% polyethelene glycol (PEG; molecular weight of 35,000), 2 µM phalloidin, and 2 µM taxol for 3 min at room temperature after a quick rinse in PBS. Cells were then fixed with 2% glutaraldehyde in PBS for at least 20 min. Fixed samples were quenched twice with 2 mg/ml $NaBH_4$ for 5–10 min, washed in PBS, and then blocked with 10% goat serum for 30 min. The primary antibodies were: rabbit polyclonal AnkG (1:100 dilution; Santa Cruz Biotechnology, Inc.), rabbit polyclonal AnkG directed to the insert region specific for the 480-kD isoform (1:100 dilution; gift from V. Bennett, Duke University, Durham, NC), rabbit spectrin βIV directed to the C terminus (1:100 dilution; gift from M. Rasband, Baylor College of Medicine, Houston, TX), mouse monoclonal pan-Neurofascin directed to the extracellular region (1:100 dilution; University of Califronia, Davis/National Institutes of Health NeuroMab Facility, Davis, CA), rabbit polyclonal NrCAM directed to the extracellular region (1:3000 dilution; Abcam), mouse monoclonal pan-Nav (1:25 dilution; Sigma-Aldrich), rabbit polyclonal α-adducin (1:100 dilution; Abcam), and mouse monoclonal TUJ1 antibody against neuron-specific tubulin β3 isoform (1:100 dilution; Covance). Secondary fluorescently labeled antibodies conjugated to Dylight (488 and 594; Jackson ImmunoResearch Laboratories, Inc.) or Alexa Flour (488, 568, and 594; Molecular Probes) were used at 1:200. For actin filament staining, Alexa Fluor 488– (1:200) or 647 (1:30)–phalloidin (Molecular Probes) was added to secondary antibody solutions. Neurons were visualized using an inverted microscope (Eclipse TE2000-U; Nikon) equipped with a Plan Apo 100× 1.3 NA objective and a charge-coupled device camera (Cascade 512B; Photometrics) driven by Metamorph imaging software (Molecular Devices).

Electron microscopy

Samples for PREM, correlative light and electron microscopy, immunogold electron microscopy, and myosin S1 decoration were processed as described previously (Svitkina, 2007, 2009). In brief, detergent-extracted samples were fixed with 2% glutaraldehyde, tannic acid, and uranyl acetate; critical point dried; coated with platinum and carbon; and transferred onto electron microscopic grids for observation. Detergent extraction to expose cytoskeletons was done as described for fluorescence microscopy. For correlative PREM, cells were cultured on glass-bottomed dishes containing coverslips that were coated with carbon through a finder grid to introduce fiducial marks, which were subsequently used to find cells imaged by fluorescence microscopy for PREM analysis. For myosin S1 decoration,

detergent-extracted unfixed cells were incubated with 0.25 mg/ml S1 in PEM buffer with 5 mM phalloidin for 30 min at room temperature and fixed with 2% glutaraldehyde. Myosin S1 (gift of Y. Goldman, University of Pennsylvania, Philadelphia, PA) was centrifuged at 100,000 *g* for 30 min before use. Gelsolin treatment to deplete actin filaments was performed as described previously (Svitkina and Borisy, 1998; Shutova et al., 2012). In brief, detergent-extracted unfixed cells were incubated with 0.4 µg/ml gelsolin (a gift of A. Weber, University of Pennsylvania, Philadelphia, PA) in buffer containing 50 mM 2-(N-morpholino)ethanesulfonic acid, pH 6.3, 2 mM $MgCl_2$, 0.1 mM $CaCl_2$, and 2 µM paclitaxel for 10 min at room temperature and fixed with 2% glutaraldehyde. For depletion of MTs, cells were first extracted with 1% Triton X-100 in PM buffer (100 mM Pipes-KOH, pH 6.9, and 1 mM $MgCl_2$) containing 2% PEG (molecular weight of 35,000) for 3 min at room temperature and then treated with prechilled PM buffer containing 0.1 M $CaCl_2$ for 45 min at 4°C. For simultaneous depletion of actin filaments and MTs, MT-depleted preparations were subsequently treated with gelsolin. For immunogold staining of AnkG, spectrin βIV, neurofascin, and NrCAM, neurons were detergent extracted, fixed with 0.2% glutaraldehyde, quenched with $NaBH_4$ for 10 min, incubated first with primary antibody (1:10 or 1:5) for 45 min, and then with 12 nm of colloidal gold–conjugated anti-rabbit or anti-mouse secondary antibody (Jackson ImmunoResearch Laboratories, Inc.) after which cells were again fixed with 2% glutaraldehyde in 0.2 M sodium cacodylate for 20 min. Immunogold staining of Nav was done similar to other AIS proteins except that the primary antibody was added after detergent extraction and before fixation; then cells were fixed, quenched, and incubated with secondary antibody. For phalloidin immunogold staining, cells were extracted as for regular PREM except that phalloidin was omitted from the extraction buffer. Then cells were fixed with 0.2% glutaraldehyde, quenched with $NaBH_4$ for 10 min, blocked with 10% donkey serum, and sequentially incubated with Alexa Fluor 488–phalloidin (1:50) for 45 min, a rabbit anti–Alexa Fluor 488 primary antibody (Molecular Probes) for 45 min, and 18 nm of colloidal gold–conjugated anti-rabbit secondary antibody (Jackson ImmunoResearch Laboratories, Inc.) after which cells were again fixed with 2% glutaraldehyde in 0.2 M sodium cacodylate for 20 min.

Samples were examined using a transmission electron microscopy (JEM 1011; JEOL USA) operated at 100 kV. Images were acquired by a charge-coupled device camera (ORIUS 832.10W; Gatan) and presented in inverted contrast. Gold particles in replica electron microscopy images were identified at high magnification after contrast enhancement to distinguish them from other bright objects in the samples. Color labeling and image overlays were performed using Adobe Photoshop (Adobe Systems), as described previously (Shutova et al., 2012).

Statistics and data analysis

Measurements were done using MetaMorph or Photoshop software packages and repeated for at least two independent experiments. Statistical analysis was performed using Excel (Microsoft) or Instat (GraphPad Software) software. Fluorescence intensities for phalloidin, adducin, and AIS proteins were determined after background subtraction. For phalloidin staining, regions containing actin-based protrusions were excluded from the analysis. For comparisons between the AIS and distal adjacent axonal regions, the position and length of the AIS was determined by AnkG immunofluorescence and the adjacent region began immediately after AnkG mean fluorescence intensity decreased by 70%. Significance was determined using two-tailed *t* tests. To determine the time course of protein accumulation in the AIS, the position of the AIS was determined by AnkG immunofluorescence and the fluorescence intensities for individual proteins were normalized to the maximal value over a period from DIV4 to DIV21. For characterizing AIS structure at different time points in vitro, neurons were categorized based on the structural features most prevalent within the middle 50% of AIS length, where the coat density was most uniform, and the percentage of neurons in each category was recorded. Actin filament orientation relative to the axon axis was determined based on S1 decoration within short (1-µm long) axon segments. Filaments oriented with their pointed end within ±45° away from or toward the cell body relative to the axon axis were assigned a distal or proximal orientation, respectively. Filaments that were not within this range were considered neutrally oriented, that is, orthogonal to the axon axis. Analysis of S1-decorated filaments excluded very short filaments accommodating less than two S1 arrowheads and long filaments at the base of actin-based protrusions, such as filopodia.

Online supplemental material

Fig. S1 shows MT bundling in the proximal axon of DIV3 neurons. Fig. S2 shows actin structures in axons of DIV3 neurons decorated with S1. Fig. S3 shows PREM of immunogold-labeled actin structures in neurons and non-neuronal cells. Fig. S4 shows how the AIS coat breaks and detaches from MTs after LatB treatment. Online supplemental material is available at http://www.jcb.org/cgi/content/full/jcb.201401045/DC1.

We thank Dr. M.A. Dichter and Ms. M. Maronski at the Neuron Culture Service Center at the University of Pennsylvania for providing hippocampal neurons, Drs. Y.E. Goldman and A. Weber for generous gifts of reagents, and Dr. V. Bennett and members of the Svitkina laboratory for helpful discussions.

This work is supported by National Institutes of Health grants GM-070898 and GM-095977 (to T. Svitkina) and training grant HD-007516 (to S.L. Jones).

The authors declare no competing financial interests.

Submitted: 13 January 2014
Accepted: 11 March 2014

References

Al-Bassam, S., M. Xu, T.J. Wandless, and D.B. Arnold. 2012. Differential trafficking of transport vesicles contributes to the localization of dendritic proteins. *Cell Rep.* 2:89–100. http://dx.doi.org/10.1016/j.celrep.2012.05.018

An, X., M. Salomao, X. Guo, W. Gratzer, and N. Mohandas. 2007. Tropomyosin modulates erythrocyte membrane stability. *Blood*. 109:1284–1288. http://dx.doi.org/10.1182/blood-2006-07-036954

Bennett, V., and A.J. Baines. 2001. Spectrin and ankyrin-based pathways: metazoan inventions for integrating cells into tissues. *Physiol. Rev.* 81:1353–1392.

Bennett, V., and J. Healy. 2009. Membrane domains based on ankyrin and spectrin associated with cell–cell interactions. *Cold Spring Harb. Perspect. Biol.* 1:a003012. http://dx.doi.org/10.1101/cshperspect.a003012

Berghs, S., D. Aggujaro, R. Dirkx Jr., E. Maksimova, P. Stabach, J.M. Hermel, J.P. Zhang, W. Philbrick, V. Slepnev, T. Ort, and M. Solimena. 2000. βIV spectrin, a new spectrin localized at axon initial segments and nodes of ranvier in the central and peripheral nervous system. *J. Cell Biol.* 151:985–1002. http://dx.doi.org/10.1083/jcb.151.5.985

Buffington, S.A., and M.N. Rasband. 2011. The axon initial segment in nervous system disease and injury. *Eur. J. Neurosci.* 34:1609–1619. http://dx.doi.org/10.1111/j.1460-9568.2011.07875.x

Byers, T.J., and D. Branton. 1985. Visualization of the protein associations in the erythrocyte membrane skeleton. *Proc. Natl. Acad. Sci. USA*. 82:6153–6157. http://dx.doi.org/10.1073/pnas.82.18.6153

Davis, J.Q., T. McLaughlin, and V. Bennett. 1993. Ankyrin-binding proteins related to nervous system cell adhesion molecules: candidates to provide transmembrane and intercellular connections in adult brain. *J. Cell Biol.* 121:121–133. http://dx.doi.org/10.1083/jcb.121.1.121

Davis, J.Q., S. Lambert, and V. Bennett. 1996. Molecular composition of the node of Ranvier: identification of ankyrin-binding cell adhesion molecules neurofascin (mucin+/third FNIII domain−) and NrCAM at nodal axon segments. *J. Cell Biol.* 135:1355–1367. http://dx.doi.org/10.1083/jcb.135.5.1355

Devaux, J.J., K.A. Kleopa, E.C. Cooper, and S.S. Scherer. 2004. KCNQ2 is a nodal K^+ channel. *J. Neurosci.* 24:1236–1244. http://dx.doi.org/10.1523/JNEUROSCI.4512-03.2004

Duflocq, A., F. Chareyre, M. Giovannini, F. Couraud, and M. Davenne. 2011. Characterization of the axon initial segment (AIS) of motor neurons and identification of a para-AIS and a juxtapara-AIS, organized by protein 4.1B. *BMC Biol.* 9:66. http://dx.doi.org/10.1186/1741-7007-9-66

Fowler, V.M. 1996. Regulation of actin filament length in erythrocytes and striated muscle. *Curr. Opin. Cell Biol.* 8:86–96. http://dx.doi.org/10.1016/S0955-0674(96)80052-4

Galiano, M.R., S. Jha, T.S. Ho, C. Zhang, Y. Ogawa, K.J. Chang, M.C. Stankewich, P.J. Mohler, and M.N. Rasband. 2012. A distal axonal cytoskeleton forms an intra-axonal boundary that controls axon initial segment assembly. *Cell*. 149:1125–1139. http://dx.doi.org/10.1016/j.cell.2012.03.039

Gallo, G. 2011. The cytoskeletal and signaling mechanisms of axon collateral branching. *Dev. Neurobiol.* 71:201–220. http://dx.doi.org/10.1002/dneu.20852

Gallo, G. 2013. Mechanisms underlying the initiation and dynamics of neuronal filopodia: from neurite formation to synaptogenesis. *Int. Rev. Cell Mol. Biol.* 301:95–156. http://dx.doi.org/10.1016/B978-0-12-407704-1.00003-8

Garrido, J.J., P. Giraud, E. Carlier, F. Fernandes, A. Moussif, M.P. Fache, D. Debanne, and B. Dargent. 2003. A targeting motif involved in sodium channel clustering at the axonal initial segment. *Science*. 300:2091–2094. http://dx.doi.org/10.1126/science.1085167

Grubb, M.S., and J. Burrone. 2010. Building and maintaining the axon initial segment. *Curr. Opin. Neurobiol.* 20:481–488. http://dx.doi.org/10.1016/j.conb.2010.04.012

Hartwig, J.H., and M. DeSisto. 1991. The cytoskeleton of the resting human blood platelet: structure of the membrane skeleton and its attachment to actin filaments. *J. Cell Biol.* 112:407–425. http://dx.doi.org/10.1083/jcb.112.3.407

Hedstrom, K.L., X. Xu, Y. Ogawa, R. Frischknecht, C.I. Seidenbecher, P. Shrager, and M.N. Rasband. 2007. Neurofascin assembles a specialized extracellular matrix at the axon initial segment. *J. Cell Biol.* 178:875–886. http://dx.doi.org/10.1083/jcb.200705119

Hedstrom, K.L., Y. Ogawa, and M.N. Rasband. 2008. AnkyrinG is required for maintenance of the axon initial segment and neuronal polarity. *J. Cell Biol.* 183:635–640. http://dx.doi.org/10.1083/jcb.200806112

Jenkins, S.M., and V. Bennett. 2001. Ankyrin-G coordinates assembly of the spectrin-based membrane skeleton, voltage-gated sodium channels, and L1 CAMs at Purkinje neuron initial segments. *J. Cell Biol.* 155:739–746. http://dx.doi.org/10.1083/jcb.200109026

Kaiser, H.W., E. O'Keefe, and V. Bennett. 1989. Adducin: Ca^{++}-dependent association with sites of cell–cell contact. *J. Cell Biol.* 109:557–569. http://dx.doi.org/10.1083/jcb.109.2.557

Kobayashi, T., B. Storrie, K. Simons, and C.G. Dotti. 1992. A functional barrier to movement of lipids in polarized neurons. *Nature*. 359:647–650. http://dx.doi.org/10.1038/359647a0

Kole, M.H., and G.J. Stuart. 2012. Signal processing in the axon initial segment. *Neuron*. 73:235–247. http://dx.doi.org/10.1016/j.neuron.2012.01.007

Kole, M.H., S.U. Ilschner, B.M. Kampa, S.R. Williams, P.C. Ruben, and G.J. Stuart. 2008. Action potential generation requires a high sodium channel density in the axon initial segment. *Nat. Neurosci.* 11:178–186. http://dx.doi.org/10.1038/nn2040

Kordeli, E., S. Lambert, and V. Bennett. 1995. AnkyrinG. A new ankyrin gene with neural-specific isoforms localized at the axonal initial segment and node of Ranvier. *J. Biol. Chem.* 270:2352–2359.

Kuhlman, P.A., C.A. Hughes, V. Bennett, and V.M. Fowler. 1996. A new function for adducin. Calcium/calmodulin-regulated capping of the barbed ends of actin filaments. *J. Biol. Chem.* 271:7986–7991.

Kusumi, A., T.K. Fujiwara, R. Chadda, M. Xie, T.A. Tsunoyama, Z. Kalay, R.S. Kasai, and K.G. Suzuki. 2012. Dynamic organizing principles of the plasma membrane that regulate signal transduction: commemorating the fortieth anniversary of Singer and Nicolson's fluid-mosaic model. *Annu. Rev. Cell Dev. Biol.* 28:215–250. http://dx.doi.org/10.1146/annurev-cellbio-100809-151736

Lemaillet, G., B. Walker, and S. Lambert. 2003. Identification of a conserved ankyrin-binding motif in the family of sodium channel α subunits. *J. Biol. Chem.* 278:27333–27339. http://dx.doi.org/10.1074/jbc.M303327200

Leterrier, C., H. Vacher, M.P. Fache, S.A. d'Ortoli, F. Castets, A. Autillo-Touati, and B. Dargent. 2011. End-binding proteins EB3 and EB1 link microtubules to ankyrin G in the axon initial segment. *Proc. Natl. Acad. Sci. USA*. 108:8826–8831. http://dx.doi.org/10.1073/pnas.1018671108

Li, X., Y. Kumar, H. Zempel, E.M. Mandelkow, J. Biernat, and E. Mandelkow. 2011. Novel diffusion barrier for axonal retention of Tau in neurons and its failure in neurodegeneration. *EMBO J.* 30:4825–4837. http://dx.doi.org/10.1038/emboj.2011.376

McEwen, D.P., and L.L. Isom. 2004. Heterophilic interactions of sodium channel β1 subunits with axonal and glial cell adhesion molecules. *J. Biol. Chem.* 279:52744–52752. http://dx.doi.org/10.1074/jbc.M405990200

McEwen, D.P., L.S. Meadows, C. Chen, V. Thyagarajan, and L.L. Isom. 2004. Sodium channel β1 subunit-mediated modulation of $Na_v1.2$ currents and cell surface density is dependent on interactions with contactin and ankyrin. *J. Biol. Chem.* 279:16044–16049. http://dx.doi.org/10.1074/jbc.M400856200

Mohandas, N., and P.G. Gallagher. 2008. Red cell membrane: past, present, and future. *Blood*. 112:3939–3948. http://dx.doi.org/10.1182/blood-2008-07-161166

Morone, N., T. Fujiwara, K. Murase, R.S. Kasai, H. Ike, S. Yuasa, J. Usukura, and A. Kusumi. 2006. Three-dimensional reconstruction of the membrane skeleton at the plasma membrane interface by electron tomography. *J. Cell Biol.* 174:851–862. http://dx.doi.org/10.1083/jcb.200606007

Moyer, J.D., R.B. Nowak, N.E. Kim, S.K. Larkin, L.L. Peters, J. Hartwig, F.A. Kuypers, and V.M. Fowler. 2010. Tropomodulin 1-null mice have a mild spherocytic elliptocytosis with appearance of tropomodulin 3 in red blood cells and disruption of the membrane skeleton. *Blood*. 116:2590–2599. http://dx.doi.org/10.1182/blood-2010-02-268458

Nakada, C., K. Ritchie, Y. Oba, M. Nakamura, Y. Hotta, R. Iino, R.S. Kasai, K. Yamaguchi, T. Fujiwara, and A. Kusumi. 2003. Accumulation of anchored proteins forms membrane diffusion barriers during neuronal polarization. *Nat. Cell Biol.* 5:626–632. http://dx.doi.org/10.1038/ncb1009

Nans, A., N. Mohandas, and D.L. Stokes. 2011. Native ultrastructure of the red cell cytoskeleton by cryo-electron tomography. *Biophys. J.* 101:2341–2350. http://dx.doi.org/10.1016/j.bpj.2011.09.050

Palay, S.L., C. Sotelo, A. Peters, and P.M. Orkand. 1968. The axon hillock and the initial segment. *J. Cell Biol.* 38:193–201. http://dx.doi.org/10.1083/jcb.38.1.193

Rasband, M.N. 2010. The axon initial segment and the maintenance of neuronal polarity. *Nat. Rev. Neurosci.* 11:552–562. http://dx.doi.org/10.1038/nrn2852

Sánchez-Ponce, D., L. Blázquez-Llorca, J. DeFelipe, J.J. Garrido, and A. Muñoz. 2012. Colocalization of α-actinin and synaptopodin in the pyramidal cell axon initial segment. *Cereb. Cortex*. 22:1648–1661. http://dx.doi.org/10.1093/cercor/bhr251

Sato, C., Y. Ueno, K. Asai, K. Takahashi, M. Sato, A. Engel, and Y. Fujiyoshi. 2001. The voltage-sensitive sodium channel is a bell-shaped molecule with several cavities. *Nature*. 409:1047–1051. http://dx.doi.org/10.1038/35059098

Shutova, M., C. Yang, J.M. Vasiliev, and T. Svitkina. 2012. Functions of nonmuscle myosin II in assembly of the cellular contractile system. *PLoS ONE*. 7:e40814. http://dx.doi.org/10.1371/journal.pone.0040814

Sloper, J.J., and T.P. Powell. 1979. A study of the axon initial segment and proximal axon of neurons in the primate motor and somatic sensory cortices. *Philos. Trans. R. Soc. Lond. B Biol. Sci.* 285:173–197. http://dx.doi.org/10.1098/rstb.1979.0004

Sobotzik, J.M., J.M. Sie, C. Politi, D. Del Turco, V. Bennett, T. Deller, and C. Schultz. 2009. AnkyrinG is required to maintain axo-dendritic polarity in vivo. *Proc. Natl. Acad. Sci. USA*. 106:17564–17569. http://dx.doi.org/10.1073/pnas.0909267106

Song, A.H., D. Wang, G. Chen, Y. Li, J. Luo, S. Duan, and M.M. Poo. 2009. A selective filter for cytoplasmic transport at the axon initial segment. *Cell*. 136:1148–1160. http://dx.doi.org/10.1016/j.cell.2009.01.016

Svitkina, T. 2007. Electron microscopic analysis of the leading edge in migrating cells. *Methods Cell Biol.* 79:295–319. http://dx.doi.org/10.1016/S0091-679X(06)79012-4

Svitkina, T. 2009. Imaging cytoskeleton components by electron microscopy. *Methods Mol. Biol.* 586:187–206. http://dx.doi.org/10.1007/978-1-60761-376-3_10

Svitkina, T.M., and G.G. Borisy. 1998. Correlative light and electron microscopy of the cytoskeleton of cultured cells. *Methods Enzymol.* 298:570–592. http://dx.doi.org/10.1016/S0076-6879(98)98045-4

Watanabe, K., S. Al-Bassam, Y. Miyazaki, T.J. Wandless, P. Webster, and D.B. Arnold. 2012. Networks of polarized actin filaments in the axon initial segment provide a mechanism for sorting axonal and dendritic proteins. *Cell Rep.* 2:1546–1553. http://dx.doi.org/10.1016/j.celrep.2012.11.015

Wilcox, K.S., J. Buchhalter, and M.A. Dichter. 1994. Properties of inhibitory and excitatory synapses between hippocampal neurons in very low density cultures. *Synapse*. 18:128–151. http://dx.doi.org/10.1002/syn.890180206

Winckler, B., P. Forscher, and I. Mellman. 1999. A diffusion barrier maintains distribution of membrane proteins in polarized neurons. *Nature*. 397:698–701. http://dx.doi.org/10.1038/17806

Xu, K., G. Zhong, and X. Zhuang. 2013. Actin, spectrin, and associated proteins form a periodic cytoskeletal structure in axons. *Science*. 339:452–456. http://dx.doi.org/10.1126/science.1232251

Zhou, D., S. Lambert, P.L. Malen, S. Carpenter, L.M. Boland, and V. Bennett. 1998. AnkyrinG is required for clustering of voltage-gated Na channels at axon initial segments and for normal action potential firing. *J. Cell Biol.* 143:1295–1304. http://dx.doi.org/10.1083/jcb.143.5.1295

Zonta, B., A. Desmazieres, A. Rinaldi, S. Tait, D.L. Sherman, M.F. Nolan, and P.J. Brophy. 2011. A critical role for Neurofascin in regulating action potential initiation through maintenance of the axon initial segment. *Neuron*. 69:945–956. http://dx.doi.org/10.1016/j.neuron.2011.02.021